Macromolecules

ARTICLE

pubs.acs.org/Macromolecules

Steric Effects in Ionic Pairing and Polyelectrolyte Interdiffusion within Multilayered Films: A Neutron Reflectometry Study

Li Xu,[†] John F. Ankner,*[,‡] and Svetlana A. Sukhishvili*[,†]

[†]Department of Chemistry, Chemical Biology and Biomedical Engineering, Stevens Institute of Technology, Hoboken, New Jersey 07030, United States

[‡]Spallation Neutron Source, Oak Ridge National Laboratory, Oak Ridge, Tennessee 37831, United States

Supporting Information

ABSTRACT: Using a series of polycations synthesized by atom transfer radical polymerization (ATRP), we investigate the effects of the polymer charge density and hydrophobicity on salt-induced interdiffusion of polymer layers within polyelectrolyte multilayer (PEM) films. Polycations with two distinct hydrophobicities and various quaternization degrees (QPDMA and QPDEA) were derived from parent polymers of matched molecular weights—poly(2-(dimethylamino)ethyl methacrylate) (PDMA) and poly(2-(diethylamino)ethyl methacrylate) (PDEA)—by quaternization with either methyl or ethyl sulfate. Multilayers of these polycations with polystyrenesulfonate (PSS) were assembled in low-salt conditions and annealed in NaCl solutions to induce layer intermixing. As revealed by neutron reflectometry (NR), polycations with lower charge density resulted in a faster decay of film structure with distance from the substrate. Interestingly, when comparing polymer mobility in QPDEA/PSS and QPDMA/PSS films, layer intermixing was faster in the case of more hydrophobic QPDEA as compared to QPDMA because of the weaker ionic pairing (due to the presence of a bulky ethyl spacer) between QPDEA and PSS.

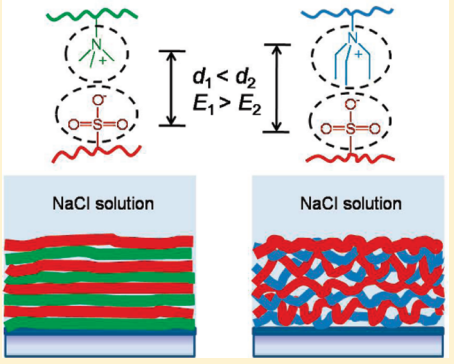

INTRODUCTION

The ability to construct highly tailored multicomponent structures enables important potential applications of polyelectrolyte multilayers (PEMs) as antibacterial coatings, drug-delivering implant coatings, optical coatings, or "smart" free-standing films.[1−7] PEMs containing strongly binding polyanions such as polystyrenesulfonate (PSS)[8] are usually considered as inherently nonequilibrium structures with polymer chains irreversibly binding to the previous layer during film layer-by-layer (LbL) deposition.[9,10] While in the case of selected strongly interacting polymer pairs (with the poly(allylamine) hydrochloride/PSS (PAH/PSS) system having the strongest interaction energy of ∼4 kT per ionic pair at room temperature[11]) the irreversible binding model might adequately describe multilayer buildup, mobility of polyelectrolytes (PEs) within the PEM and chain exchange with solution have increasingly been reported. For example, significant chain mobility can occur within these films following exposure to salts. Atomic force microscopy (AFM) measurements have revealed smoothening of PEM surfaces after exposure of LbL films in salt solutions,[12,13] and polymer diffusion in the direction parallel to the substrate was detected by fluorescence recovery after pattern photobleaching (FRAPP).[14,15] Moreover, in some cases polymer chains can diffuse through PEM films and exchange with the solution phase. For example, fluorescently labeled poly(L-lysine) (PLL) chains diffuse throughout the entire film thickness during deposition of PLL/hyaluronan PEMs.[16,17] In other examples, exchange and/or displacement of polymer chains preassembled within either hydrogen-bonded or electrostatically assembled PEM films by polymer chains invading from solution have been detected using *in situ* ATR-FTIR.[18−20]

While polymer chain mobility within multilayer films can sometimes be beneficially used to construct thicker films and/or to induce surface self-assembly of biological objects (such as viruses),[21,22] polymer intermixing often compromises potential applications of PEMs that rely on internal film structuring. One example of such an application is multistage, multidrug delivery of therapeutic compounds from LbL films. Indeed, with low-charge-density PEs, including biologically relevant and/or natural polymers, difficulties have been met in engineering a sequential release of PEM-incorporated functional therapeutic compounds, and clay platelets[23,24] or strongly associating PEs need to be incorporated into LbL films to separate consecutive multilayer components and obtain film stratification.[25−31] While the strategy of barrier layers has been partially successful, improved understanding of PE mobility can enable better structural control over PEMs.

As with polyelectrolyte complexes (or polyplexes) in solution,[32−34] mobility of polymer chains within PEMs is affected

Received: April 29, 2011
Revised: June 10, 2011
Published: July 22, 2011

by several factors which modulate inter-polyelectrolyte binding. For example, the transition from the linear to the exponential growth regime, commonly associated with increased polymer intermixing, can be controlled by the solution pH,[21,35] polymer molecular weight and/or polydispersity,[36] or the type of small ions used in the deposition solutions.[37] The type of small ions and the total ionic strength of solutions were both found to strongly affect the lateral mobility of assembled PE chains.[14] Among various factors, the PE charge density has been identified as one of the most important parameters controlling polymer lateral diffusion[14] and postassembly exchange between assembled polymers and polymer chains in solution.[38] For example, enhanced interdiffusion and solution−film exchange were observed only if the degree of ionization of polyamine species was lower than 70%.[38]

Neutron reflectometry (NR) is uniquely suited for studies of internal layering in PEM films. The technique was initially applied to a strongly bound PAH/PSS system.[39,40] PAH/PSS films with marker layers of deuterated PSS (dPSS) showed regular Bragg peaks and an internal interfacial root-mean-square (rms) roughness σ comparable to PAH or PSS layer thicknesses.[39,40] Several studies reported an increase in σ when low-molecular-weight salt was introduced into the system during self-assembly[39,40] or as a postassembly step.[41] In an elegantly simple model of two-stack films of protonated and deuterated polyelectrolytes, Helm and coworkers have recently determined that the internal roughness of PEMs changes with the distance from the film surface, indicating that progressive polyelectrolyte interdiffusion occurs during film dipping cycles.[42] An increase in internal roughening in PAH/PSS multilayer films was also induced by heating the deposition solutions.[43,44] Our group has recently reported more diffuse polymer layering for weak PEs[45] and hydrogen-bonded polymers[46] within LbL films. Interestingly, as with an earlier NR study of the structure of amphoteric, highly conjugated sulfonated poly(aniline)/PAH films,[47] we also found that interfacial widths increased with distance from the substrate.[45,46] When comparing NR results between these different systems, it is logical to draw a correlation between the value of σ and its decay at distances away from a solid surface and the strength of intermolecular interactions.

Using NR, Jomaa and Schlenoff demonstrated an increase in the interfacial roughness of poly(diallyldimethylammonium) (PDADMAC)/PSS multilayers and eventually complete polymer intermixing in PEMs during annealing in salt solutions.[41] Here, we study the dependence of salt-induced mobility of PEs within PEMs on the PE charge density, chain hydrophobicity, and steric restrictions to ionic pairing. While the effects of these parameters have been explored for polyelectrolyte complexes,[48,49] the roles of these parameters in internal layering of PEMs and salt-induced chain intermixing remain largely unexplored. One interesting recent observation, for example, is enhanced interdiffusion within the film of PDADMAC/PSS strong polyelectrolytes as compared to PAH/PSS films.[42] In this work, using polycations (PCs) with systematically varied charge density, backbone hydrophobicity, and steric hindrance to ionic pairing, we construct PC/PSS films with periodically inserted dPSS marker layers and use NR to probe variations in the PEM internal structure during film exposure to salt solutions. We demonstrate that PE charge density significantly affects not only the absolute value of the internal film roughness σ but also its variation with distance from the substrate. Importantly, in experiments on salt-annealing of PEMs, we show that steric restrictions to the ion-to-ion spacing in PE pairing can be more important than PE backbone hydrophobicity for the mobility of polymer chains within LbL films.

EXPERIMENTAL SECTION

Materials. 2-(Dimethylamino)ethyl methacrylate and 2-(diethylamino)ethyl methacrylate were purchased from Aldrich. Ultrapure Milli-Q water (Millipore) with a resistivity of ∼18 MΩ/cm was used in all experiments. Polystyrenesulfonate, sodium salt (PSS), with M_w = 77 000 g mol^{-1} and polydispersity index (PDI) ∼1.20 and branched polyethylenimine (BPEI) with M_w = 25 000 g mol^{-1} and PDI = 2.50 were purchased from Aldrich. Deuterated polystyrenesulfonate, sodium salt (dPSS), with M_w = 55 800 g mol^{-1} and PDI = 1.03 was purchased from Polymer Source, Inc. One-side-polished silicon wafers of 4 in. diameter with ⟨100⟩ orientation and resistivity 0.001−0.005 Ω·cm were purchased from the Institute of Electronic Materials Technology (Poland). All other chemicals were purchased from Aldrich and used without further purification.

Polymer Synthesis and Characterization. Poly(2-(dimethylamino)ethyl methacrylate) (PDMA) and poly(2-(diethylamino)ethyl methacrylate) (PDEA) homopolymers were synthesized by atom transfer radical polymerization (ATRP) which has been described elsewhere.[50,51] Briefly, PDMA was polymerized using ethyl 2-bromoisobutyrate (EBiB), CuBr, and 1,1,4,7,10,10-hexamethyltriethylenetetramine (HMTETA) with a molar ratio of monomer:EBiB:CuBr:HMTETA of 150:1:1:2 at room temperature in 8 mL of 2-propanol. The polymerization was allowed to proceed under continuous stirring in an argon atmosphere for 12 h. The reaction was terminated with liquid nitrogen and diluted with THF. The catalyst complex was removed by passage through a basic aluminum oxide column. After removal of most of the THF solvent, the concentrated solution was precipitated into cold hexane, and the obtained polymers were dried in a vacuum oven at 30 °C overnight. The weight-average molecular weights of PDMA and PDEA homopolymers were 30 kDa, as determined by a combination of gel permeation chromatography (GPC) and ^{1}H NMR. The GPC studies performed in THF revealed PDI = 1.10 and 1.18 for PDMA and PDEA, respectively.

Quantitative quaternization of PDMA and PDEA homopolymers was carried out at room temperature.[52−54] PDMA homopolymer was dissolved in a mixture of (v:v = 1:3) methanol and benzene, followed by dropwise addition of a stoichiometric amount of dimethyl sulfate needed to achieve the required degree of quaternization. The mixture was stirred at room temperature overnight. Quaternized PDMA polymers (QPDMAs) were then precipitated with ethanol/THF three times and washed with acetone several times. The quaternization of PDEA to obtain QPDEA polymers was carried out using diethyl sulfate. Figure 1 shows the synthesis and quaternization procedures for QPDMA and QPDEA polycations.

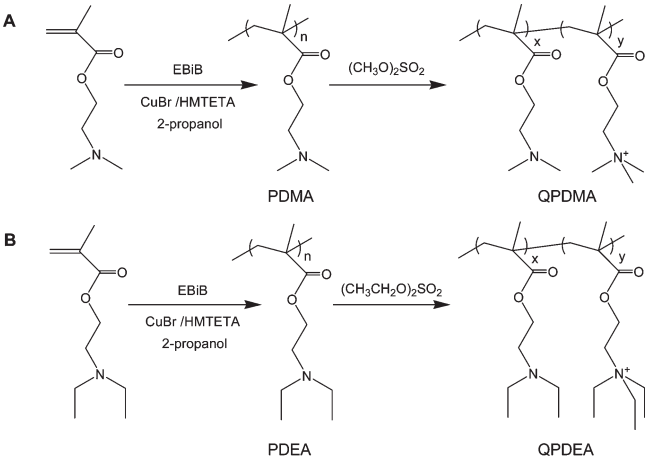

Figure 1. Reaction scheme for the synthesis and quaternization of (A) PDMA and (B) PDEA homopolymers.

The extent of quaternization was determined by ^{1}H NMR spectroscopy in D_2O at pH 9. For example, Figure 2a shows the ^{1}H NMR spectrum of the PDMA homopolymer in D_2O at pH 9. The peak C at δ 2.3−2.5 ppm represents the dimethylamino protons in DMA residues. After quaternization with dimethyl sulfate, peak F at 3.3−3.4 ppm appeared, indicating quaternization of dimethylamino group. Integrals of peaks C and F were used to determine the degree of quaternization of the homopolymer (Figure 2b,c). In Figure 2d, the absence of dimethylamino protons at 2.3−2.4, 2.8, and 4.3 ppm (peaks C, B, and A, respectively) indicates 100% quaternization degree. Six polycations with matched quaternization degrees (10%, 40%, and 100%) are abbreviated as Q10M, Q40M, and Q100M for QPDMAs and Q10E, Q40E, and Q100E for QPDEAs, respectively.

Multilayer Deposition. Quaternized polyelectrolytes (QPEs) and PSS were dissolved in 0.01 M tris(hydroxymethyl)aminomethane (TRIS) buffer solution at pH 9. The silicon wafers were cleaned as described elsewhere.[46] Multilayer buildup started with the absorption of BPEI at pH 4 for 15 min, followed by the assembly of 24-bilayer films of BPEI/PSS/$[(QPE/PSS)_4/(QPE/dPSS)]_4/(QPE/PSS)_4$ from 0.2 mg/mL solutions by LbL self-assembly. Deuterated PSS was deposited with every fifth bilayer to provide neutron scattering contrast. All solutions were controlled at pH 9 and room temperature. Multilayer films were fabricated by dipping silicon substrates in PSS solution for 15 min, followed by rinsing with 0.01 M TRIS buffer solution for 2 min. The PSS-topped substrates were subsequently dipped in QPE solution for 15 min and again rinsed with TRIS buffer solution twice for 2 min. This process was repeated until the desired number of layers had been deposited. The samples were blow-dried with dry nitrogen, kept for 1 week exposed to ambient air, and measured at Oak Ridge National Lab (ORNL).

Ellipsometry. Measurements of dry multilayer thicknesses were performed using a custom-built, single-wavelength, phase-modulated ellipsometer at 65° angle of incidence. The refractive indices for the native silicon oxide layer and dry multilayer films on a silicon substrate were set at 1.456 and 1.500, respectively. The thicknesses of each layer were measured after being blow-dried by nitrogen flow.

Atomic Force Microscopy (AFM). An NSCRIPTOR dip pen nanolithography system (Nanoink) operating in the AFM mode was used to characterize dry polycations/PSS films. AFM was operated in the contact mode using P-MAN-SICT-0 AFM cantilevers (Pacific Nanotechnology, Inc.) with a nominal force constant of 0.2 N/m.

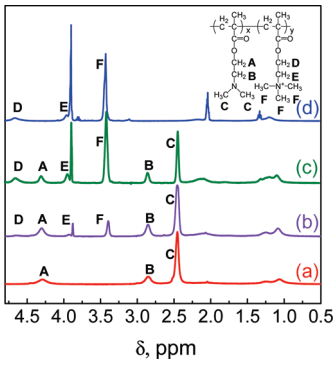

Figure 2. ^{1}H NMR spectra of (a) unquaternized PDMA, (b) Q10M, (c) Q40M, and (d) Q100M polycations measured in D_2O at pH 9.

Neutron Reflectometry. Neutron reflectivity measurements were performed in the Spallation Neutron Source Liquids Reflectometer (SNS-LR) in ORNL.[55] The reflectivity data were collected in a continuous wavelength band (2.5 Å < λ < 5.75 Å), at a sequence of different incident angles: θ = 0.15, 0.25, 0.45, 0.65, 0.85, 1.60, and 2.80°. The momentum transfer, $Q = (4\pi \sin \theta/\lambda)$, was varied in the range of 0.006 Å^{-1} < Q < 0.245 Å^{-1}. The reflectivity curves were collected by combining the six different angle data sets together, and the constant instrument resolution was maintained at $\delta Q/Q$ = 0.05 for all six angles by varying the incident-beam apertures.

The NR data collected on the interdiffusion of layer-by-layer films were analyzed using a model developed for NR studies of hydrogen-bonded multilayers.[46] Since the material in individual PE layers typically extends over several nominal bilayer thicknesses (as determined by the total amount of material deposited) and the scattering densities of the protonated PSS and quaternized polymers are similar, we average the protonated-layer scattering densities and model the dPSS markers as immersed in this average protonated material. After annealing in salt solution, diffusion in these films can be tracked by the dispersion of dPSS marker layers into the protonated matrix. Thicknesses, scattering densities, and interlayer diffusion widths were modified iteratively until the reflectivity curve was best fitted (minimize χ^2). Interdiffusion of layers was modeled as "limited source diffusion".[41,56] In cases of extreme diffusion of deuterated marker layers (diffusion width equal to adjacent marker and matrix layer widths), layer thicknesses and diffusion width are held constant and the scattering density contrast reduced, consistent with the diffusion.[57]

Calculations of Steric Hindrance Using Stable Geometries of the Functional Groups in QPEs. To simplify the calculation, we treated QPDMA as $N^+(CH_3)_3(CH_2CH_3)$, QPDEA as $N^+(CH_2CH_3)_4$, and PSS as $CH_3SO_3^-$. The stable geometries of the charged pairs of $N^+(CH_3)_3(CH_2CH_3)/CH_3SO_3^-$ and $N^+(CH_2CH_3)_4/CH_3SO_3^-$ were modeled using Gaussian 98 ab initio calculations.[58] The calculations were carried out by Hartree−Fock SCF method, using the 6-31G split-valence basis set in the Gaussian orbital wave functions. A gradient method was adopted in the program for geometry optimizations.

RESULTS AND DISCUSSION

Film Buildup and Internal Structure. Deposition of the QPDMA/PSS and QPDEA/PSS multilayers on silicon wafers with BPEI/PSS precursor layers was first measured by ellipsometry. Growth curves for six polymer systems are shown in Figure S1 of the Supporting Information. To prevent protonation of unquaternized polycation units (pK_a values are 6.6 and 6.9 for PDMA and PDEA, respectively[59]), films were deposited from polymer solutions at pH 9. All films exhibited a linear increase in film thickness as a function of layer number. The individual thicknesses differed significantly for PCs of various charge densities (Table 1). For both QPDMA/PSS and QPDEA/PSS multilayer types, the film thickness and assembled amount for QPE decreased with the degree of quaternization, which is in agreement with previous layer-by-layer deposition experiments.[60−62] According to the charge-compensation mechanism

Table 1. Average Values and Standard Deviations for Dry Ellipsometric Thicknesses of Bilayers within QPDMA/PSS and QPDEA/PSS Films

multilayer films	QPDMA/PSS			QPDEA/PSS		
polycations	Q10M	Q40M	Q100M	Q10E	Q40E	Q100E
$d_{bilayer}$ (nm)	6.7 ± 0.8	3.7 ± 0.8	2.1 ± 0.5	11.3 ± 0.7	4.3 ± 0.8	3.1 ± 0.6

dx.doi.org/10.1021/ma200986d |Macromolecules 2011, 44, 6518–6524

of adsorption, for polymer chains with lower charge density, a larger amount of material should be adsorbed onto the oppositely charged layer to achieve the same surface charge and form thicker, loopy-conformation layers.

We then aimed to explore the internal structure of PEM films containing QPDMA or QPDEA polymers using NR. Our hypothesis was that polycation hydrophobicity should affect the propensity of polyelectrolytes to intermix during film deposition and therefore should be reflected in the PEM internal film structure. Hydrophobicity of polycations of PDMA and PDEA types was estimated using the octanol:water partition coefficient (log *P*) of the corresponding monomers. Values of log *P* (shown in Table S1 of the Supporting Information) for unquaternized PDMA and PDEA as well as for quaternized polycations were calculated by nine computational methods provided by ALOGPS 2.1 of Advanced Chemical Development Inc.: ALOGPs, ACLogP, AB/LogP, miLogP, ALOGP, MLOGP, KOWWIN, XLOGP2, and XLOGP3.[63,64] While in the case of Q100M and Q100E different methods gave widely varying log *P* values that could not be utilized to determine the hydrophobicity of the quaternized polyelectrolyte chains (data not shown), all nine techniques were consistent in estimating the hydrophobicity of unquaternized PDMA and PDEA (Table S1 in Supporting Information). Specifically, the average values of log *P* were 1.00 ± 0.28 for PDMA and 1.84 ± 0.22 for PDEA, indicating greater hydrophobicity of PDEA and therefore of QPDEA polycations.

Figure 3 shows neutron reflectivity data of QPDMA/PSS and QPDEA/PSS 24-bilayer films with dPSS marker layers deposited in each fifth bilayer. The left panels represent experimental neutron reflectivity *R* plotted as a function of momentum transfer *Q*, and the right panels show the scattering density profile used to produce the solid lines shown with the reflectivity data.[46] The film structural parameters (scattering densities, thicknesses, and internal roughnesses) are summarized in Tables S2−S4 of the Supporting Information. The overall film thicknesses obtained from NR were ∼10−30% thinner than the ellipsometric values (Table S4 in Supporting Information), most likely due to differences in ambient film hydration during the respective measurements. For all six as-deposited films, NR data could not be fitted unless the thicknesses of deuterated marker layers significantly exceeded their nominal values determined from average total film thickness. The marker-layer scattering densities were diluted by protonated matrix material in inverse proportion to their broadening to conserve mass. We therefore infer that chain intermixing occurs during the PEM dipping steps. Similarly, a large degree of polyelectrolyte intermixing has been seen in our earlier work on multilayers of weak PEs[45] and hydrogen-bonded LbL films.[46] Figure 3 shows that for both QPDMA/PSS and QPDEA/PSS systems the PE charge density has a dramatic effect on stratification of PEMs throughout the entire film thickness. While Q100M/PSS and Q100E/PSS films can be modeled assuming well-defined and regularly spaced marker layers, films of PEs with lower charge densities—Q10s and Q40s—could not be fitted with simple uniform, periodic internal structural profiles. The internal structure of the latter films decays with distance from the substrate. This accumulated disorder results from easier chain intermixing for PCs with low charge densities. When comparing PDMA- and PDEA-based polyelectrolytes of the same quaternization degree, faster decay of the film structure with distance from the substrate is observed with Q10E/PSS as compared to Q10M/PSS films, with four deuterated marker layer thicknesses (*d*) of 55, 69, 70, and 85 Å (starting from the substrate) and 71, 80.9, 191, and 242 Å for Q10M/PSS and Q10E/PSS films, respectively (Tables S2 and S3 in the Supporting Information). However, this can be a consequence of

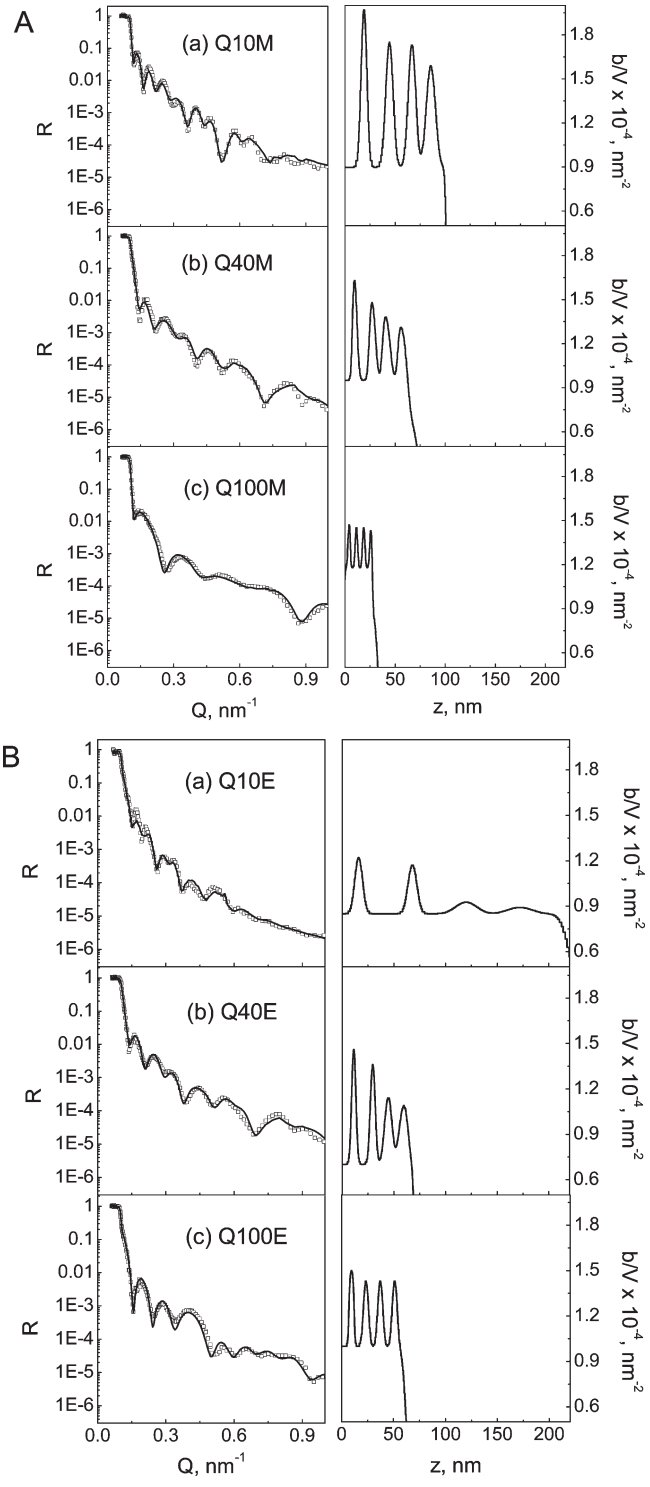

Figure 3. Plot of reflectivity *R* vs *Q* (left) and the corresponding scattering length density profile (right) of dry (A) BPEI/PSS/$[(QPDMAs/PSS)_4/(QPDMAs/dPSS)]_4/(QPDMAs/PSS)_4$ and (B) BPEI/PSS/$[(QPDEAs/PSS)_4/(QPDEAs/dPSS)]_4/(QPDEAs/PSS)_4$ films with degrees of quaternization of (a) 10%, (b) 40%, and (c) 100%, respectively. The deposition of the films was carried out in 0.01 M pH 9 TRIS buffer solutions at 25 °C.

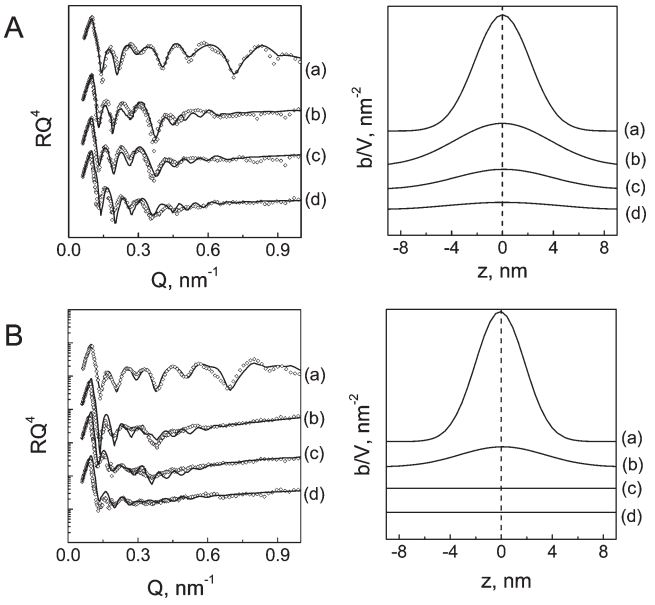

Figure 4. Neutron reflectivity data (left) and corresponding scattering length density profiles (plotted as $R \times Q^4$ to enhance small features) (right) for the closest-to-the-substrate dPSS layer of dry (A) BPEI/PSS/$[(Q40M/PSS)_4/(Q40M/dPSS)]_4/(Q40M/PSS)_4$ and (B) BPEI/PSS/$[(Q40E/PSS)_4/(Q40E/dPSS)]_4/(Q40E/PSS)_4$ PEMs after annealing in 1.6 M NaCl for (a) 0, (b) 2, (c) 6, and (d) 12 h.

the greater individual layer thicknesses in the case of Q10E-containing films. With Q40M/PSS and Q40E/PSS films with the same number of layers and individual layer thicknesses, the diffused dPSS layer thicknesses d, and their evolution with distance from the substrate were instead similar to each other (47, 59, 78, 95 Å and 38, 55, 75, 90 Å for Q40M/PSS and Q40E/PSS films, respectively (Tables S2 and S3)) within ~15% accuracy of the fitting procedure and thickness variation associated with manual deposition of multilayers. Keeping in mind that QPDMA and QPDEA PEs were quaternized with methyl and ethyl groups, respectively, and that these groups might affect QPE hydrophobicity, as well as impose steric restriction during polyelectrolyte pairing, we then explored the relative contributions of PE hydrophobicity and steric hindrance to ionic pairing on chain interdiffusion in PEMs. Note that enhanced hydrophobicity is often considered to strengthen interpolyelectrolyte chain interactions.[49]

Salt-Induced Interdiffusion of Polymers with Matched Charge Densities and Chain Lengths. To induce interdiffusion of PE within PEMs, we used the salt annealing technique previously reported by Schlenoff and co-workers.[20] Our choice of polymer pair and the optimal concentration of salt for PEM structural annealing were guided by our results on film stability and internal structure as revealed by ellipsometry and NR, respectively. The use of 0.8 M NaCl solutions to anneal film structure was not suitable, as Q10M/PSS and Q10E/PSS PEMs both decomposed after a 5 min exposure to these solutions (as indicated by ellipsometry), while no structural changes were observed in NR data of Q40M/PSS, Q40E/PSS, Q100M/PSS, and Q100E/PSS films even after 1 week of annealing in these solutions (data not shown). In contrast, the use of 1.6 M NaCl solution induced rearrangements of the Q40M/PSS and Q40E/PSS film structure on a time scale of hours.

Figure 4 shows the neutron reflectivity and scattering length density profiles for the closest-to-the-substrate dPSS layer of Q40M and Q40E PEMs upon exposure to 1.6 M NaCl solutions. In both cases, with greater time of annealing, the definition of the features in the neutron reflectivity curves decreases, showing the loss of the well-defined lamellar structure in the as-assembled films. The fitted scattering length density profiles reveal increasing intermixing of marker and matrix material with salt immersion time. On the basis of an ion-pairing model at the surface[20] as well as in solution,[65] the movement of oppositely charged polyelectrolyte chains results from the introduction of ion-pairing between residual salt ions and the charged groups in the polymer chains. Before annealing, the polymer chains are strongly paired to oppositely charged units through multiple ionic interactions. Hence, the movement of the chain requires the dissociation of the bonding pair of two oppositely charged units to overcome the potential barrier imposed by electrostatic pairing of polyelectrolyte chains. Upon exposure to the highly concentrated salt solution, the extrinsic salt ions replace a fraction of the polymer−polymer ionic pairs, decreasing the energy barrier to polymer mobility.[41]

Interestingly, slower rearrangements of the structure were observed in Q40M PEMs than in Q40E-containing films. Upon annealing for 2−12 h, gradual interdiffusion is seen in the Q40M/PSS films. In contrast, with Q40E/PSS, we observe near complete intermixing of film components after 6 h (Figure 4B). The ~10% increase in the dry thickness after salt annealing as determined from NR likely results from NaCl in the films.[66] Importantly, AFM images of Q40M/PSS and Q40E/PSS PEMs in Figure S2 show that the rms roughness at the film−air interface remained at ~6 ± 1 and ~4 ± 0.5 nm before and after 48 h annealing in 1.6 M NaCl, respectively, confirming that evolution of NR profiles reflected internal layer intermixing.

While the degree of polymer intermixing is dependent on the distance from the substrate of the deuterated marker layers in the Q40/PSS films (as shown in Figure 3), here we consider the diffusion coefficients of QPDMA/PSS and QPDEA/PSS films calculated from the spreading rate of the closest-to-the-substrate dPSS marker layers. Note that for all polymer systems diffusion coefficients were similar (within 25%) for the 2nd and 3rd marker layers farther from the substrate (data not shown). A comparison of the diffusion coefficients for the closest and furthest marker layers from the substrate is given in Figure S3 of the Supporting Information. Assuming that diffusion of polymer chains in a direction vertical to the substrate follows a Gaussian distribution, the diffusion coefficient of dPSS within the multilayer films can be calculated using the "limited source diffusion" model:[41,56]

$$C(x,t) = \frac{Q_0}{(4\pi Dt + 2\pi{\sigma_0}^2)^{1/2}} e^{-x^2/(4Dt + 2{\sigma_0}^2)} \quad (1)$$

where $C(x,t)$ is the concentration of the deuterated polymer (mol/cm^3) at distance x from the peak maximum of the marker layer at time t and σ_0 is the width of the initial layer, obtained from the Gaussian fitting of scattering density profile of the deuterated layer in the as-deposited film. From Figure 4, the values of σ_0 were 4.34 and 3.85 nm for the closest-to-the-substrate dPSS layer of Q40M and Q40E PEMs, respectively. Q_0 in eq 1 is the amount of dPSS (measured by the scattering density) deposited in the deuterated layer, and D is the diffusion coefficient of dPSS. Assuming that D remains constant during the

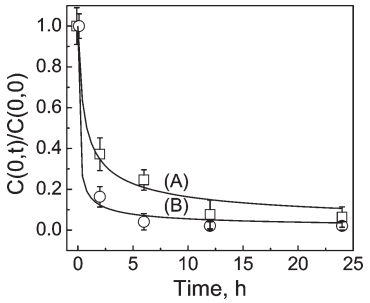

Figure 5. Plot of relative dPSS concentration at the peak maximum in scattering length density profile vs annealing time for the closest-to-the-substrate dPSS layer of (A) Q40M/PSS and (B) Q40E/PSS multilayer films. The corresponding fitting is obtained using eq 2. D is taken from the fitting of NR curves, and σ_0 is obtained from the Gaussian fitting of the peaks.

Table 2. ESBE in $N^+(CH_3)_3(CH_2CH_3)/CH_3SO_3^-$ and $N^+(CH_2CH_3)_4/CH_3SO_3^-$ Pairs Calculated by Gaussian 98 Using Hartree−Fock SCF Modeling and 6-31G Split-Valence Basis Set

ionic pair	$N^+(CH_3)_3(CH_2CH_3)/CH_3SO_3^-$	$N^+(CH_2CH_3)_4/CH_3SO_3^-$
ESBE (au)	−0.1581	−0.1480

entire salt-annealing process, we have

$$\frac{C(0,t)}{C(0,0)} = \frac{\sigma_0}{(2Dt + \sigma_0^2)^{1/2}} \quad (2)$$

Plots of relative dPSS concentration at the peak maximum of profile vs diffusion time for the closest-to-the-substrate dPSS layer within Q40M/PSS and Q40E/PSS multilayers are given in Figure 5. The values of D_{dPSS} were obtained through fitting the plots of dPSS concentration vs diffusion time using eq 2. The fitting in Figure 5A yields D_{dPSS} for the closest-to-the-substrate dPSS layer of Q40M/PSS PEMs as $(9 \pm 1) \times 10^{-17}$ cm^2 s^{-1}. This value is ∼3-fold greater than D_{dPSS} of 2.9×10^{-17} cm^2 s^{-1} measured in PDADMA/PSS films annealed in 0.8 M NaCl[41] and ∼12−18 times larger than the results obtained by Soltwedel et al. for diffusion of polymer chains in PDADMA/PSS PEMs during film deposition from polymer solutions that additionally contained 0.1 M NaCl.[42] The slower PE intermixing in the earlier reported cases is probably due to the lower salt concentrations used with PEMs[42] as well as to differences in polyelectrolyte type.

Important differences are seen between the interdiffusion rates in Q40M/PSS and Q40E/PSS systems (Figure 5). In particular, D_{dPSS} for the closest-to-the-substrate dPSS layer of Q40E/PSS PEMs calculated from Figure 5B was $(6 \pm 1) \times 10^{-16}$ cm^2 s^{-1} which is ∼7-fold larger than that of dPSS in the Q40M/PSS system. Note that both Q40M and Q40E polycations remained soluble in solutions of 1.6 M NaCl. This significant difference in mobility of PE within PEM films results from the steric bulk of the ethyl groups at the quaternary nitrogen of Q40E. The stable geometries for the charged group pairs of $N^+(CH_3)_3(CH_2CH_3)/CH_3SO_3^-$ and $N^+(CH_2CH_3)_4/CH_3SO_3^-$ calculated by Gaussian 98 using Hartree−Fock SCF modeling and the 6-31G split-valence basis set are shown in Figure S4 of the Supporting Information. The electrostatic binding energies (ESBE) for two pairs are summarized in Table 2. The binding energy in $N^+(CH_3)_3(CH_2CH_3)/CH_3SO_3^-$ pairs was larger than that in $N^+(CH_2CH_3)_4/CH_3SO_3^-$ pairs, which supports the hypothesis that steric bulk around the amino group enlarges the distance between oppositely charged groups. The consequence of such steric hindrance is a weaker ESBE between oppositely charged layers in QDEA PEMs and an increased distance between amino group in QPDEA chains and sulfonate group in PSS chains.

In addition, it is also interesting to compare the salt-annealing rates for polymers with different charge densities. Figure S5 in the Supporting Information shows the NR curves of the closest-to-the-substrate dPSS layer of dry Q100M/PSS PEMs annealed in 1.6 M NaCl buffer solution at pH 9 on a time scale of hours. Fitting the scattering length density distribution of the closest-to-the-substrate dPSS peak in Q100M/PSS films with a Gaussian profile gave σ_0 of 2.24 nm. From the time evolution of the relative dPSS concentration at the center of the layer and the modeling shown above, D_{dPSS} of $(3 \pm 0.6) \times 10^{-17}$ cm^2 s^{-1} was obtained for the Q100M/PSS system. This value is ∼3-fold smaller than that for the diffusion of the polyelectrolyte within Q40M/PSS multilayers containing a lower charge density polycation Q40M. This observation is consistent with other reports on the important role of polyelectrolyte charge density in polymer chain dynamics.[14,38] The slower diffusion of PE of higher charge density is also consistent with the data in Figure 3 of this paper showing more reluctant intermixing in PEMs with strongly charged QPEs.

In summary, we have studied the influence of the ionization of polyelectrolytes and steric hindrance on growth and postdeposition salt annealing of PEMs. NR studies show that PEMs of high-charge-density PEs have low internal roughness and exhibit high retention of periodic layered structure with distance from the substrate as compared to their low-charge-density counterparts. Interestingly, in experiments on salt-annealing of PEMs with polyelectrolytes with matched charge densities, steric hindrance effects were found to be a more important factor than the overall chain hydrophobicity in determining the internal structure and mobility of the polyelectrolyte chains. Polyelectrolytes with higher steric hindrance to ionic pairing were more prone to chain intermixing and formed more diffuse, interpenetrated PEMs during annealing in salt solutions.

■ ASSOCIATED CONTENT

Ⓢ Supporting Information. Fitting parameters of neutron reflectivity. This material is available free of charge via the Internet at http://pubs.acs.org.

■ AUTHOR INFORMATION

Corresponding Author

*E-mail: anknerjf@ornl.gov (J.F.A.); ssukhish@stevens.edu (S.A.S.).

■ ACKNOWLEDGMENT

We thank Aliaksandr Zhuk (Stevens Institute of Technology) for his help with NR measurements and Thomas Cattabiani and Dr. Yong Zhang (Stevens Institute of Technology) for their useful discussions. We are also thankful to Bo Liu (Stony Brook University) for his help with Gaussian 98 ab initio calculations. This work was supported by the National Science Foundation under Award DMR-0906474. The neutron measurements were

performed at the Spallation Neutron Source at the Oak Ridge National Laboratory, managed by UT-Battelle, LLC, for the DOE under Contract DE-AC05-00OR22725.

REFERENCES

(1) Wang, T. C.; Cohen, R. E.; Rubner, M. F. *Adv. Mater.* **2002**, *14*, 1534.
(2) Lichter, J. A.; Van Vliet, K. J.; Rubner, M. F. *Macromolecules* **2009**, *42*, 8573.
(3) Hammond, P. T. *Adv. Mater.* **2004**, *16*, 1271.
(4) Peyratout, C. S.; Dähne, L. *Angew. Chem., Int. Ed.* **2004**, *43*, 3762.
(5) Cranston, E. D.; Gray, D. G. *Biomacromolecules* **2006**, *7*, 2522.
(6) Fu, J. H.; Ji, J.; Yuan, W. Y.; Shen, J. C. *Biomaterials* **2005**, *26*, 6684.
(7) Aulin, C.; Johansson, E.; Wågberg, L.; Lindström, T. *Biomacromolecules* **2010**, *11*, 872.
(8) Decher, G. *Science* **1997**, *277*, 1232.
(9) Schlenoff, J. B.; Ly, H.; Li, M. *J. Am. Chem. Soc.* **1998**, *120*, 7626.
(10) Dubas, S. T.; Schlenoff, J. B. *Macromolecules* **1999**, *32*, 8153.
(11) Jaber, J. A.; Schlenoff, J. B. *Langmuir* **2007**, *23*, 896.
(12) Dubas, S. T.; Schlenoff, J. B. *Langmuir* **2001**, *17*, 7725.
(13) McAloney, R. A.; Dudnik, V.; Goh, M. C. *Langmuir* **2003**, *19*, 3947.
(14) Nazaran, P.; Bosio, V.; Jaeger, W.; Anghel, D. F.; von Klitzing, R. *J. Phys. Chem. B* **2007**, *111*, 8572.
(15) Jourdainne, L.; Lecuyer, S.; Arntz, Y.; Picart, C.; Schaaf, P.; Senger, B.; Voegel, J.-C.; Lavalle, P.; Charitat, T. *Langmuir* **2008**, *24*, 7842.
(16) Picart, C.; Mutterer, J.; Richert, L.; Luo, Y.; Prestwich, G. D.; Schaaf, P.; Voegel, J.-C.; Lavalle, P. *Proc. Natl. Acad. Sci. U.S.A.* **2002**, *99*, 12531.
(17) Lavalle, P.; Picart, C.; Mutterer, J.; Gergely, C.; Reiss, H.; Voegel, J.-C.; Senger, B.; Schaaf, P. *J. Phys. Chem. B* **2004**, *108*, 635.
(18) Kharlampieva, E.; Sukhishvili, S. A. *Macromolecules* **2003**, *36*, 9950.
(19) Kharlampieva, E.; Sukhishvili, S. A. *Langmuir* **2004**, *20*, 10712.
(20) Jomaa, H. W.; Schlenoff, J. B. *Langmuir* **2005**, *21*, 8081.
(21) Yoo, P. J.; Zacharia, N. S.; Doh, J.; Nam, K. T.; Belcher, A. M.; Hammond, P. T. *ACS Nano* **2008**, *2*, 561.
(22) Yoo, P. J.; Nam, K. T.; Qi, J.; Lee, S.-K.; Park, J.; Belcher, A. M.; Hammond, P. T. *Nature Mater.* **2006**, *5*, 234.
(23) Glinel, K.; Laschewsky, A.; Jonas, A. M. *Macromolecules* **2001**, *34*, 5267.
(24) Vuillaume, P. Y.; Jonas, A. M.; Laschewsky, A. *Macromolecules* **2002**, *35*, 5004.
(25) Zacharia, N. S.; DeLongchamp, D. M.; Modestino, M.; Hammond, P. T. *Macromolecules* **2007**, *40*, 1598.
(26) Boulmedais, F.; Bozonnet, M.; Schwinte, P.; Voegel, J.-C.; Schaaf, P. *Langmuir* **2003**, *19*, 9873.
(27) Garza, J. M.; Schaaf, P.; Muller, S.; Ball, V.; Stoltz, J.-F.; Voegel, J.-C.; Lavalle, P. *Langmuir* **2004**, *20*, 7298.
(28) Garza, J. M.; Jessel, N.; Ladam, G.; Dupray, V.; Muller, S.; Stoltz, J.-F.; Schaaf, P.; Voegel, J.-C.; Lavalle, P. *Langmuir* **2005**, *21*, 12372.
(29) Jourdainne, L.; Arntz, Y.; Senger, B.; Debry, C.; Voegel, J.-C.; Schaaf, P.; Lavalle, P. *Macromolecules* **2007**, *40*, 316.
(30) Mertz, D.; Hemmerle, J.; Mutterer, J.; Ollivier, S.; Voegel, J.-C.; Schaaf, P.; Lavalle, P. *Nano Lett.* **2007**, *7*, 657.
(31) Wood, K. C.; Chuang, H. F.; Batten, R. D.; Lynn, D. M.; Hammond, P. T. *Proc. Natl. Acad. Sci. U.S.A.* **2006**, *103*, 10207.
(32) Kovacevic, D.; Van der Burgh, S.; de Keizer, A.; Cohen Stuart, M. A. *Langmuir* **2002**, *18*, 5607.
(33) Pristinski, D.; Kozlovskaya, V.; Sukhishvili, S. A. *J. Chem. Phys.* **2005**, *122*, 014907.
(34) Mjahed, H.; Voegel, J.-C.; Chassepot, A.; Senger, B.; Schaaf, P.; Boulmedais, F.; Ball, V. *J. Colloid Interface Sci.* **2010**, *346*, 163.
(35) Fu, J.; Ji, J.; Shen, L.; Kuller, A.; Rosenhahn, A.; Shen, J.; Grunze, M. *Langmuir* **2009**, *25*, 672.
(36) Sun, B.; Jewell, C. M.; Fredin, N. J.; Lynn, D. M. *Langumir* **2007**, *23*, 8452.
(37) Wong, J. E.; Zastrow, H.; Jaeger, W.; von Klitzing, R. *Langmuir* **2009**, *25*, 14061.
(38) Zacharia, N. S.; Modestino, M.; Hammond, P. T. *Macromolecules* **2007**, *40*, 9523.
(39) Schmitt, J.; Grünewald, T.; Decher, G.; Pershan, P. S.; Kjaer, K.; Lösche, M. *Macromolecules* **1993**, *26*, 7058.
(40) Lösche, M.; Schmitt, J.; Decher, G.; Bouwman, W. G.; Kjaer, K. *Macromolecules* **1998**, *31*, 8893.
(41) Jomaa, H. W.; Schlenoff, J. B. *Macromolecules* **2005**, *38*, 8473.
(42) Soltwedel, O.; Ivanova, O.; Nestler, P.; Müller, M.; Köhler, R.; Helm, C. A. *Macromolecules* **2010**, *43*, 7288.
(43) Gopinadhan, M.; Ivanova, O.; Ahrens, H.; Günther, J.-U.; Steitz, R.; Helm, C. A. *Macromolecules* **2005**, *38*, 5228.
(44) Gopinadhan, M.; Ivanova, O.; Ahrens, H.; Günther, J.-U.; Steitz, R.; Helm, C. A. *J. Phys. Chem. B* **2007**, *111*, 8426.
(45) Kharlampieva, E.; Ankner, J. F.; Rubinstein, M.; Sukhishvili, S. A. *Phys. Rev. Lett.* **2008**, *100*, 128303.
(46) Kharlampieva, E.; Kozlovskaya, V.; Ankner, J. F.; Sukhishvili, S. A. *Langmuir* **2008**, *24*, 11346.
(47) Kellogg, G. J.; Mayes, A. M.; Stockton, W. B.; Ferreira, M.; Rubner, M. F. *Langmuir* **1996**, *12*, 5109.
(48) San Juan, A.; Letourneur, D.; Izumrudov, V. A. *Bioconjugate Chem.* **2007**, *18*, 922.
(49) Filippov, S. K.; Koňák, Č.; Kopečková, P.; Starovoytova, L.; Špírková, M.; Štdpánek, P. *Langmuir* **2010**, *26*, 4999.
(50) Zhang, X.; Xia, J. H.; Matyjaszewski, K. *Macromolecules* **1998**, *31*, 5167.
(51) Xu, L.; Zhu, Z. C.; Borisov, O. V.; Zhulina, E. B.; Sukhishvili, S. A. *Phys. Rev. Lett.* **2009**, *103* (11), 118301.
(52) Petzhold, C. L.; Stefens, J.; Monteavaro, L. L.; Stadler, R. *Polym. Bull.* **2000**, *44*, 477.
(53) Deboubt, K.; Delporte, M.; Loucheux, C. *Macromol. Chem. Phys.* **1995**, *196*, 303.
(54) Bütün, V.; Armes, S. P.; Billingham, N. C. *Macromolecules* **2001**, *34*, 1148.
(55) Kharlampieva, E.; Kozlovskaya, V.; Chan, J.; Ankner, J. F.; Tsukruk, V. V. *Langmuir* **2009**, *25*, 14017.
(56) Walpole, R. E.; Myers, H. R.; Myers, S. L. *Probability and Statistics for Engineers and Scientists*; Prentice Hall: Englewood Cliffs, NJ, 1998.
(57) Crank, J. *The Mathematics of Diffusion*, 2nd ed.; Oxford University Press: New York, 1975.
(58) Frisch, M. J.; Trucks, G. W.; Schlegel, H. B.; Gill, P. M. W.; Johnson, B. G.; Robb, M. A.; Cheeseman, M. J. R.; Keith, T. A.; Petersson,G. A.; Montgomery, J. A.; Raghavachari, K.; Al-Laham, M. A.; Zakrzewski, V. G.; Ortiz, J. V.; Foresman, J. B.; Ciosloswki, J.; Stefanof, B. B.; Nanayakkara, A.; Challacombe, M.; Peng, C. Y.; Ayala, P. Y.; Chen, W.; Wong, M. W.; Andres, J. L.; Replogle, E. S.; Gomperts, R.; Martin, R. L.; Fox, D. J.; Binkley, J. S.; Defrees, D. J.; Baker, J.; Stewart, J. P.; Head-Gordon, M.; Gonzalez, C.; Pople, J. A. *Gaussian 98, Revision A.7*; Gaussian, Inc.: Pittsburgh, PA, 1998.
(59) Lee, A. S.; Gast, A. P.; Bütün, V.; Armes, S. P. *Macromolecules* **1999**, *32*, 4302.
(60) van de Steeg, H. G. M.; Cohen Stuart, M. A.; de Keizer, A.; Bijsterbosch, B. H. *Langmuir* **1992**, *8*, 2538.
(61) Böhmer, M. R.; Heesterbeek, W. H. A.; Deratani, A.; Renard, E. *Colloids Surf., A* **1995**, *99*, 53.
(62) Kharlampieva, E.; Sukhishvili, S. A. *Langmuir* **2003**, *19*, 1235.
(63) VCCLB, Virtual Computational Chemistry Laboratory. VCCLAB, Virtual Computational Chemistry Labroatory; http://www.vcclab.org, 2005.
(64) Livingston, D. J. *Curr. Top. Med. Chem.* **2003**, *3*, 1171.
(65) Kabanov, V. A. *Polym. Sci.* **1994**, *36*, 143.
(66) Farhat, T. R.; Schlenoff, J. B. *J. Am. Chem. Soc.* **2003**, *125*, 4627.